Applied Acoustics 180 (2021) 108109

Contents lists available at ScienceDirect

Applied Acoustics

journal homepage: www.elsevier.com/locate/apacoust

Spontaneous catastrophe behaviour in acoustic black holes at low frequencies

Xiao Liang [a,b], Jiaming Chu [a,b], Jiale Tan [a,b], Songhui Nie [a,b], Baixi Liu [a,b], Xuejun Zheng [a,b], Zhuo Zhou [c,*], Jiu Hui Wu [c,*]

[a] Xiangtan University School of Mechanical Engineering, Xiangtan 411105, China
[b] Foshan Green Intelligent Manufacturing Research Institute of Xiangtan University, Guangdong 528311, China
[c] School of Mechanical Engineering and State Key Laboratory for Strength and Vibration of Mechanical Structures, Xi'an Jiaotong University, Xi'an, Shanxi 710049, China

ARTICLE INFO

Article history:
Received 2 September 2020
Received in revised form 3 April 2021
Accepted 6 April 2021

Keywords:
Acoustic black hole
Catastrophe behaviour
Landau's phase-transition theory

ABSTRACT

In acoustic black holes (ABH) at low frequencies, catastrophe sound energy flux behaviour occurs spontaneously if the tip size of the ABHs reaches a critical value. This report demonstrates that this catastrophe behaviour can be quantified by analysing the relative phase transitions using Landau's phase-transition theory. Two catastrophe behaviours corresponding to two stable phases (states) were observed using analytical calculations and a numerical analysis. The sound energy flux was proportional to 3 power laws and square relationships with the tip diameters, respectively. The 3 power law relationships were proved using low-frequency experimental observations. For engineering applications, ABH structures with small tip diameters can isolate more than 11 dB of low-frequency sound waves below 1600 Hz. We associated this cataclysmic phase transition with the geometric structure of the ABHs.

1. Introduction

The transport process of acoustic energy flux in ABHs is an outstanding phase-transition process whose theoretical description is far from complete [1–4]. ABHs were first applied to beams, which can manipulate bending waves to capture their energy by changing the structure's thickness in the form of a power function ($y = A(x)^m$). Bending wave deceleration in ABHs was also discovered. The wave velocity tends to be zero at the end of ABHs without reflection [5]. Subsequent experiments showed that the catastrophe energy flux sharply decreased at the small tips of ABHs [6]. Slow waves and sound energy-focusing effects also occur when sound waves propagate in ABHs, which influences the absorption of sound waves in ABHs [7,8]. The slow wave effect also gives ABHs good absorption effects on sound waves in water, significantly expanding the application of ABHs in absorbing waves [9]. From the phase-transition perspective, slow waves and energy-focusing effects in ABHs are catastrophe behaviours that occur spontaneously as tip sizes in ABHs change, and sound energy-focusing effects have also been found in ABHs, which make sound insulation and absorption possible [10–12]. A double-leaf acoustic black hole beam was proposed to expand the low-frequency range of sound absorption [13]. The reflection properties of ABHs were studied via an experimental method, demonstrating that the reflection coefficient of the designed ABHs could be reduced by more than 50% at low frequencies due to the acoustic behaviour of two-dimensional ABHs at low frequencies, similar to a simple hole with no scattering and reflection but exhibited scattering effects at high frequencies [14–16].

Although phase transitions and catastrophe behaviour in ABHs have been observed, there is no theoretical description or quantitative relationships between the stable phases in this phase-transition process. Understanding this process is extremely important to reveal the nature of ABH sound transmission and its applications.

We used Landau's phase-transition theory to investigate spontaneous catastrophe behaviour in ABHs and the quantitative relationships under stable phases. Landau's phase-transition theory is the present focus of research into phase transitions [17–19]. This subject lies at the intersection of two important concepts: on the one hand, statistical mechanics and mathematical methods are used to describe the spontaneous catastrophe behaviour and gradients in phase transitions of systems [20–22]. On the other hand, some concepts and tools developed in the phase-transition field are used to analyse complex non-equilibrium systems [22–24]. Therefore, Landau's phase-transition theory can be used as an

* Corresponding authors.
E-mail addresses: zhouzhuo221@163.com (Z. Zhou), ejhwu@mail.xjtu.edu.cn (J.H. Wu).

https://doi.org/10.1016/j.apacoust.2021.108109
0003-682X/

advantageous tool to analyse spontaneous catastrophe behaviour of sound energy flux in ABHs.

In this paper, we propose a phase-transition model to analyse spontaneous catastrophe behaviour in ABHs. Using Landau's phase-transition theory, we build a theoretical model to investigate the catastrophe behaviour of acoustic energy flux in different phases of ABHs in Section 2. In Section 3, the quantitative relationships of each stable phase are studied and verified via numerical simulations. We also verify our theoretical results on the quantitative relationship using experiments in Section 4.

2. Methods

ABHs are similar to funnel structures with decreasing diameters, forming a tip at the exit as shown in Fig. 1. The functional expression of the diameter d at length x is as follows:

$$d = Ax^m + \frac{d_0}{2} \tag{1}$$

where A is the expansion index, m is the exponential parameter, x is the length, $0 \le x \le L$, and d_0 is the tip diameter.

At low frequencies, a small tip diameter causes sound waves to decelerate, producing sound energy-focusing effects [5,7], and catastrophe changes in the sound energy flux appear spontaneously. The critical value d_c of the tip diameter is used to determine these catastrophe changes. When $d_0 > d_c$, sound waves flow from the entrance of ABHs and can completely flow from their outlet tips. However, when $d_0 < d_c$, not all acoustic waves can flow from the tip of ABHs, causing sound energy-focusing effects, which trigger catastrophe changes in the acoustic energy flux. Acoustic energy-focusing behaviour is a typical non-equilibrium phase transition, and the two stable phases are distinguished by the critical diameter d_c.

Non-equilibrium phase transitions occurring in various ways in applied sciences are important to engineers and scientists [25]. We used Landau's phase-transition theory to establish a mathematical model for the phase-transition process in ABHs at low frequencies. According to an analysis of reports in the literature [5,7], a small tip diameter d_0, a change rate in the wave velocity $\partial v/\partial t$ related to wave deceleration in ABHs, and the parameters related to acoustic energy flux, sound energy E, sound velocity c, and medium density ρ are important physical parameters that determine catastrophe behaviour in ABHs and phase transitions [5,7,26]. Therefore, a potential function Φ that can describe transitions in ABHs is their function, that is, $\Phi = f(\rho, \partial v/\partial t, c, E, d_0)$.

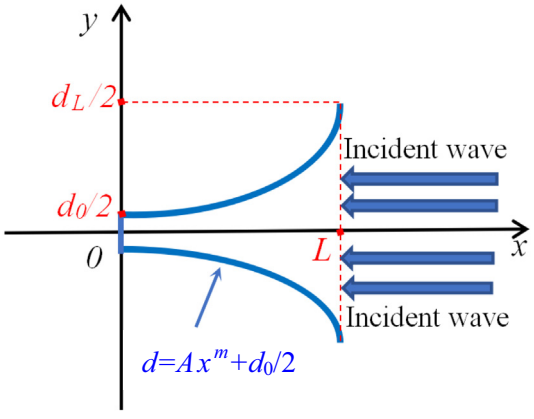

Fig. 1. ABH structural model according to Eq. (1) (colour online).

$$\Phi\left(\rho, \frac{\partial v}{\partial t}, c, E, \eta\right) = \Phi_0 + t(\rho, \frac{\partial v}{\partial t}, E, c)\eta^2 + \frac{1}{2}u(\rho, \frac{\partial v}{\partial t}, E, c)\eta^4 \tag{2}$$

where t and u are the functions of ρ, $\partial v/\partial t$, c, and E, and η is the order parameter that denotes the macroscopic physical properties or structures of a system after and before phase transitions that describe the system's phase transitions. Catastrophe phase transitions occur when the critical top diameter d_c is reached [18]. Therefore, the order parameter η is $\eta = d_0\text{-}d_c$.

Fig. 2 shows the distribution of the potential function Φ in Eq. (2) when $t \ge 0$ and $t < 0$. When $t \ge 0$, the system only has a stable phase when $\eta = 0$, that is, $d = d_c$, and when $d \ne d_c$, the system is unstable (black and red lines in Fig. 2). When $t < 0$, the system has two stable phases when $\eta = \pm(-t/u)^{1/2}$ (red points in Fig. 2) and an unstable phase when $\eta = 0$ (green point in Fig. 2) [23].

In a stable equilibrium state, the potential function Φ should be the minimum and satisfy [25]:

$$\partial\Phi/\partial\eta = 2t\eta + 2u\eta^3 = 0 \tag{3}$$

We obtain $\eta = 0$ or $\eta = \pm(-t/u)^{1/2}$ using Eq. (3). For sound energy flux of ABHs at low frequencies, the stable phase occurs when $d \ne d_c$, and the critical dimension d_c is a critical point for distinguishing the two stable phases. Therefore, $t < 0$ and $\eta = d\text{-}d_c = \pm(-t/u)^{1/2}$. Constructing the t and u functions is the key to researching catastrophe phase transitions in ABHs and the quantitative relationships between the two stable phases. Eq. (3) demonstrates that t and u should satisfy $\eta = d\text{-}d_c = \pm(-t/u)^{1/2}$, and for catastrophe sound energy flux in ABHs, we can construct a simple power-law function using the parameters ρ, $\partial v/\partial t$, c, and E to describe the catastrophe phase transitions of sound energy flux in ABHs.

$$(d - d_c)^2 = -\frac{t}{u} = a\rho^{\alpha_1}\left(\frac{\partial v}{\partial t}\right)^{\alpha_2} c^{\alpha_3} E^{\alpha_4} \tag{4}$$

where a is a constant and a greater than 0. According to Landau's phase-transition theory, u is considered a constant [22]. Thus, the following relationship is obtained:

$$(d - d_c)^2 = -\frac{a\rho^{\alpha_1}(\partial v/\partial t)^{\alpha_2} c^{\alpha_3} E^{\alpha_4}}{u} = b\rho^{\alpha_1}\left(\frac{\partial v}{\partial t}\right)^{\alpha_2} c^{\alpha_3} E^{\alpha_4} \tag{5}$$

where $b = -a/u$.

Using a dimensionless analysis, we further reduce the number of power exponents of the parameters ρ, $\partial v/\partial t$, c and E. Note that $d\text{-}d_c$ has $[L]$ dimensions, and the dimensions of ρ, $\partial v/\partial t$, c, and E are $[L]^{-2}[M]^1$, $[L]^1[T]^{-2}$, $[L]^1[T]^{-1}$, and $[L]^2[T]^{-2}[M]^1$, respectively. To satisfy Eq. (5), the dimensions of $\rho^{\alpha_1}(\frac{\partial v}{\partial t})^{\alpha_2} c^{\alpha_3} E^{\alpha_4}$ should be $[L]^2$,

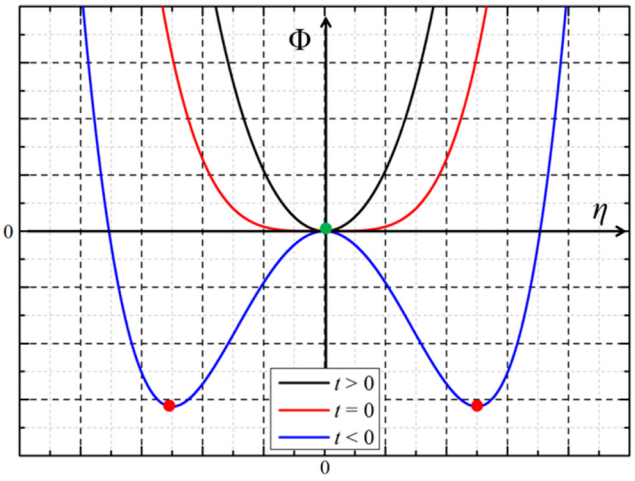

Fig. 2. Distribution of the potential function Φ when $t > 0$, $t = 0$, and $t < 0$ (colour online).

and the exponents obtained using the dimensional analysis are related as shown in Table 1.

The following relationships between the exponents are derived:

$$\begin{cases} -2\alpha_1+\alpha_2+\alpha_3+2\alpha_4=2 \\ -2\alpha_2-\alpha_3-2\alpha_4=0 \\ \alpha_1+\alpha_4=0 \end{cases} \Rightarrow \begin{cases} \alpha_1=-\alpha_4 \\ \alpha_2=2-2\alpha_4 \\ \alpha_3=4-6\alpha_4 \end{cases} \tag{6}$$

Eqs. (4) and (6) are used to obtain the expression of t:

$$t=a\rho^{-\alpha_4}\left(\frac{\partial v}{\partial t}\right)^{(2-2\alpha_4)}c^{4-6\alpha_4}E^{\alpha_4} \tag{7}$$

Substituting Eq. (7) into Eq. (2), we obtain:

$$\Phi\left(\rho,\left(\frac{\partial v}{\partial t}\right),c,E,\eta\right)=\Phi_0+a\rho^{-\alpha_4}\left(\frac{\partial v}{\partial t}\right)^{(2-2\alpha_4)}c^{4-6\alpha_4}E^{\alpha_4}\eta^2+\frac{1}{2}u\eta^4 \tag{8}$$

The power index α_4 in the potential function Eq. (8) is an important parameter that determines the phase transitions and catastrophe behaviour in ABHs. Using Eq. (8), we draw a graph of the relationship among the potential function Φ, the order parameter $\eta = d\text{-}d_c$, and the power index α_4 when $\Phi_0 = 0$ as shown in Fig. 3.

There are two critical values of $\alpha_4 = 2/3$ and $\alpha_4 = 1$ where the potential function Φ has two minima and a maximum value when the order parameter $d\text{-}d_c = 0$, which shows that there are two stable phases and one unstable phase. As demonstrated in Fig. 3 (a) and (b), when $\alpha_4 = 2/3$, the order parameter $k\text{-}k_c = 0$ is an extremely unstable critical point, the system is in an unstable phase, and this unstable phase spontaneously and rapidly reaches the adjacent stable phase. In ABHs, when the tip diameter decreases d and equals the critical diameter d_c, it moves from stable phase 1 to a critical state, and a small decrease near the d_c point causes the spontaneous transfer to another stable phase 2 as shown in the red line in Fig. 3(a) and (b). When the tip diameter d crosses the critical diameter d_c while decreasing, it is a spontaneously catastrophe behaviour from stable phase 1 to stable phase 2 that corresponds to the first-order phase transition (or discontinuous phase transition) in Landau's phase-transition theory as shown by the blue lines in Fig. 3(a) and (b).

As demonstrated in Fig. 3(c), a similar catastrophe phase transition is also observed at $\alpha_4 = 1$, which is easier to assess using logarithmic coordinates.

3. Quantitative relationships of different phases in ABHs

To obtain the phase-transition process in ABHs and further reveal the quantitative relationships between these parameters in each stable phase using Eqs. (5) and (7), the order parameter η is:

$$\eta=(d-d_c)^2=b\rho^{-\alpha_4}\left(\frac{\partial v}{\partial t}\right)^{(2-2\alpha_4)}c^{4-6\alpha_4}E^{\alpha_4} \tag{9}$$

The sound energy E is obtained from Eq. (9):

$$E=b^{-\frac{1}{\alpha_4}}\cdot\rho^{1}\cdot\left(\frac{\partial v}{\partial t}\right)^{\frac{2\alpha_4-2}{\alpha_4}}\cdot c^{\frac{6\alpha_4-4}{\alpha_4}}\cdot(d-d_c)^{\frac{2}{\alpha_4}} \tag{10}$$

Using Landau's phase-transition theory, the first-order phase transition is regarded as catastrophe sound energy flux in ABHs caused by the sound energy-focusing effect incited by wave deceleration that is induced by a decrease in the diameter. Therefore, the extreme point of this first-order phase transition can be solved using the first partial derivative of E when the other parameters ($\partial v/\partial t$ and c) are zero [23], that is, $\partial E/(\frac{\partial v}{\partial t}) = 0$ and $\frac{\partial E}{\partial c} = 0$. Of note, when $\frac{\partial E}{\partial(d-d_c)} = 0$ and $\frac{\partial E}{\partial b} = 0$, α_4 is infinite and Eq. (10) will diverge, so it has no practical significance. We calculate that $\alpha_4 = 1$ and $\alpha_4 = 2/3$, respectively. Bringing $\alpha_4 = 1$ and $\alpha_4 = 2/3$ into Eq. (10), we obtain

$$E=b^{-1}\cdot\rho\cdot c^2\cdot(d-d_c)^2 \tag{11}$$

$$E=b^{-\frac{3}{2}}\cdot\rho\cdot\left(\frac{\partial v}{\partial t}\right)\cdot(d-d_c)^3 \tag{12}$$

Eqs. (11) and (12) describe the quantitative relationships of the two stable phases in the sound energy catastrophe flux and phase-transition process. The sound energy E is proportional to the tip diameter d to the square relation (d^2) and the 3 power law (d^3). Eqs. (11) and (12) can also be deduced using the first partial derivative of η when $\partial v/\partial t$ and c are zero, that is, $\partial\eta/(\frac{\partial v}{\partial t}) = 0$ and $\frac{\partial \eta}{\partial c} = 0$.

To study the behaviour of the catastrophe flux in ABHs and quantitative relationships between the two stable phases, a 3D ABH finite element model is developed via the acoustic solid coupling module in COMSOL software, which is used to calculate the transmission coefficient under different tip diameters as shown in Figs. 4 and 5.

As shown in Fig. 4, the inlet diameters $d_L = D$ of the simulated ABHs are 100 mm. The tip diameters are 1 mm, 10 mm, 12 mm, 30 mm, 60 mm, 66 mm, 70 mm, and 80 mm in Fig. 4(a)–(h), respectively. The incident wave is a plane wave. We simulate the sound field distribution in these ABH and calculate the ratios of the transmitted sound energy E_t to the incident sound energy E_i to obtain the sound insulation characteristics and analyse the catastrophe and quantitative relationships in the phase-transition process using the sound field distribution.

As shown in Fig. 4(a)–(c), for small tip diameters whose tip diameter ratios to inlet diameter d/D are only 0.01, 0.10, and 0.12, the sound energy-focusing effect can be clearly observed. The sound pressure at the tip is much greater than that at the inlet, which can be seen from the sound pressure contours. However, as the tip diameter increases to 30, the sound energy-focusing effect persists but is not very obvious. The sound pressure contours indicate that the difference between the tip sound pressure and the inlet sound pressure is smaller, indicating that the sound energy-focusing effect weakens as the tip diameter increases as shown in Fig. 4(d). When $d/D = 0.6$, the sound energy-focusing effect becomes extremely weak, and the sound pressure difference between the inlet and outlet is only 0.8 Pa. The catastrophe acoustic energy flux appears until $d/D = 0.66$, where there is almost no sound pressure, which indicates that the sound wave completely passes through the ABHs as demonstrated in Fig. 4(e) and (f). When $d/D > 0.66$ ($d/D = 0.7$ and $d/D = 0.8$), the situation is almost the same when $d/D = 0.66$ as shown in Fig. 4(g) and (h).

We also calculated the transmission coefficient of the simulated ABHs as shown in Fig. 5. Note that the sound transmission coefficient t_w is the ratio of the sound energy transmitted out from ABHs' E_t to the incident sound energy E_i, which is expressed as [16]:

Table 1
Relationships between ρ, $\partial v/\partial t$, c, E, and $\eta = d\text{-}d_c$.

	P (α_1)	$\partial v/\partial t$ (α_2)	c (α_3)	E (α_4)	$H = d\text{-}d_c$
L	−2	1	1	2	2
T	0	−2	−1	−2	0
M	1	0	0	1	0

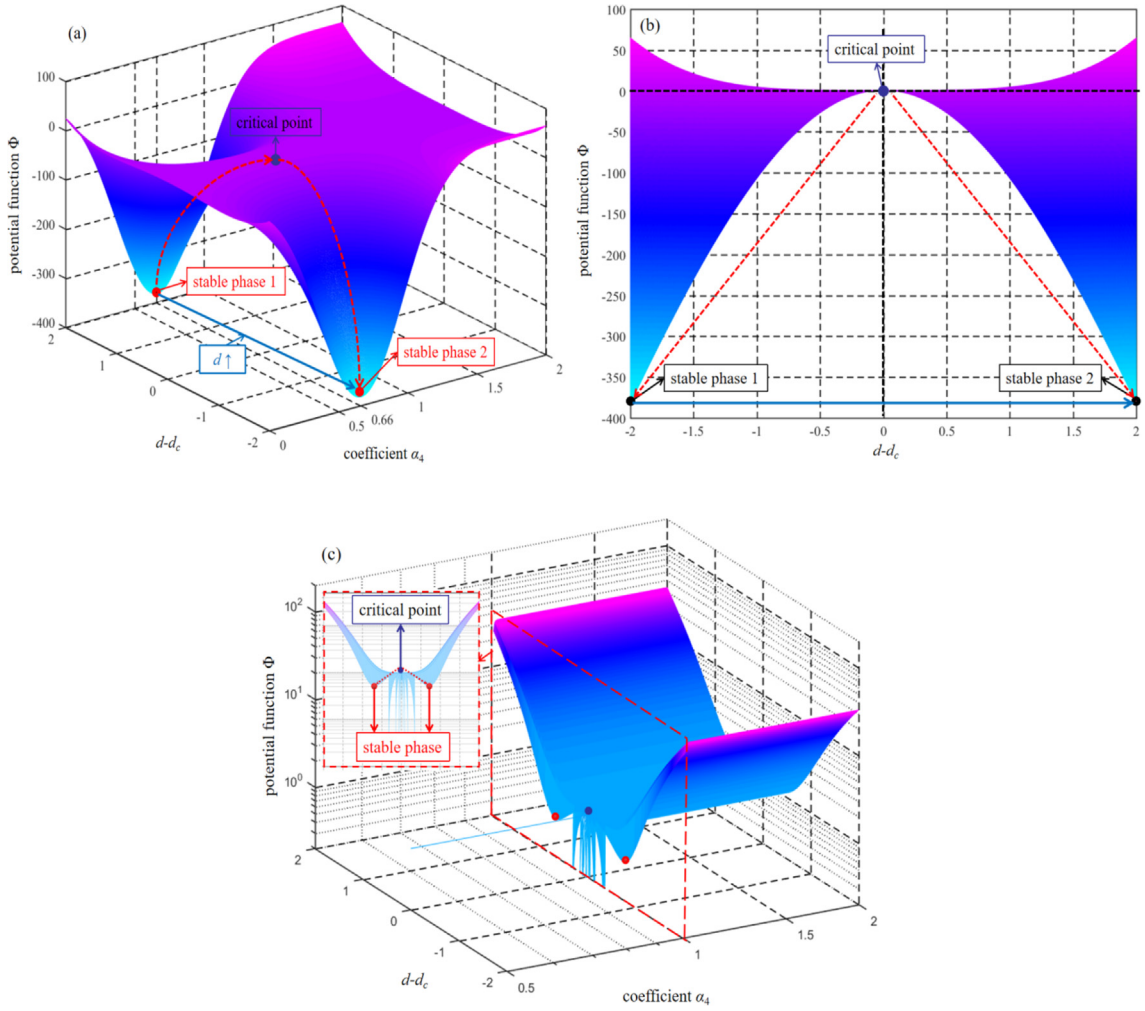

Fig. 3. The relationship between the potential function Φ, order parameter $\eta = d\text{-}d_c$, and power index α_4 (colour online).

$$t_w = \frac{E_t}{E_i} = \left(\frac{P_t}{P_i}\right)^2 \tag{13}$$

where E_t is the average sound energy density of transmitted waves, $E_t = P_t^2/2\rho_0 c_0$, P_t is the sound pressure of transmitted waves, E_i is the average sound energy density of incident sound waves, $E_i = P_i^2/2\rho_0 c_0$, and P_i is the sound pressure of incident waves.

The transmission coefficient t_w increases as the ABH tip diameter increases, reaching 100% at $d/D = 0.7$ as shown in Fig. 5. For low-frequency sound waves, decreasing the tip diameter can significantly reduce the transmission coefficient. When the tip diameter is <1 mm, the low-frequency transmission coefficient is close to 0, which means that almost all of the sound waves are localised within ABHs.

To explore the catastrophe and quantitative relationship between transmission coefficient t_w and tip diameter d, we calculated the relationships between the transmission coefficient t_w and tip diameter d at different frequencies (50 Hz, 100 Hz, 200 Hz, and 300 Hz) through simulation results as shown in Fig. 6. The spontaneous catastrophe sound energy in ABHs occurs at $d/D = 0.66$ as demonstrated in Fig. 6(a) and (b), which is consistent with the simulation results.

To calculate the relationship between the transmission coefficient t_w and tip diameter d in our model as shown in Eq. (13), we assume that the transmitted sound energy E_t is equal to the sound energy E in our theoretical model, that is, $E_t = E$. Thus, the sound transmission coefficients of ABHs are:

$$t_w = \left(\frac{P_t}{P_i}\right)^2 = \frac{E_t}{E_i} = \frac{E}{E_i} = \frac{b^{-1}\rho c^2 d^2}{E_i} = Ad^2 \tag{14}$$

and

$$t_w = \left(\frac{P_t}{P_i}\right)^2 = \frac{E_t}{E_i} = \frac{E}{E_i} = \frac{b^{-2/3}\rho(\partial v/\partial t)d^3}{E_i} = B(\partial v/\partial t)d^3 \tag{15}$$

where A is a constant, A = b-1ρc2/Ei, B is a constant, and B = b - 2/3ρ/Ei, so, in the first and second stable phases, the sound transmission coefficient tw is proportional to d2 and d3, respectively.

As shown in Fig. 6(b), when $d/D \leq 0.3$, the transmission coefficient tw is proportional to the 3 power law of the tip diameter d, that is, tw~d3. When $0.3 \leq d/D \leq 0.5$, the square relationship between the transmission coefficient tw and tip diameter d (tw~d2) is observed. This simulation result fully verifies our theoretical results.

4. Experimental validation

To verify the quantitative relationship obtained using our theoretical method, a sound experiment is conducted on a standing wave tube. The sound transmission loss (*STL*) of samples #1, #2, and #3 is measured using a BK4206 standing wave tube. As shown in Fig. 7, the inlet diameters of the three samples are 99 mm. The tip diameters of samples #1, #2, and #3 are 12 mm, 14 mm, and 20 mm, respectively, and the lengths of three acoustic black holes

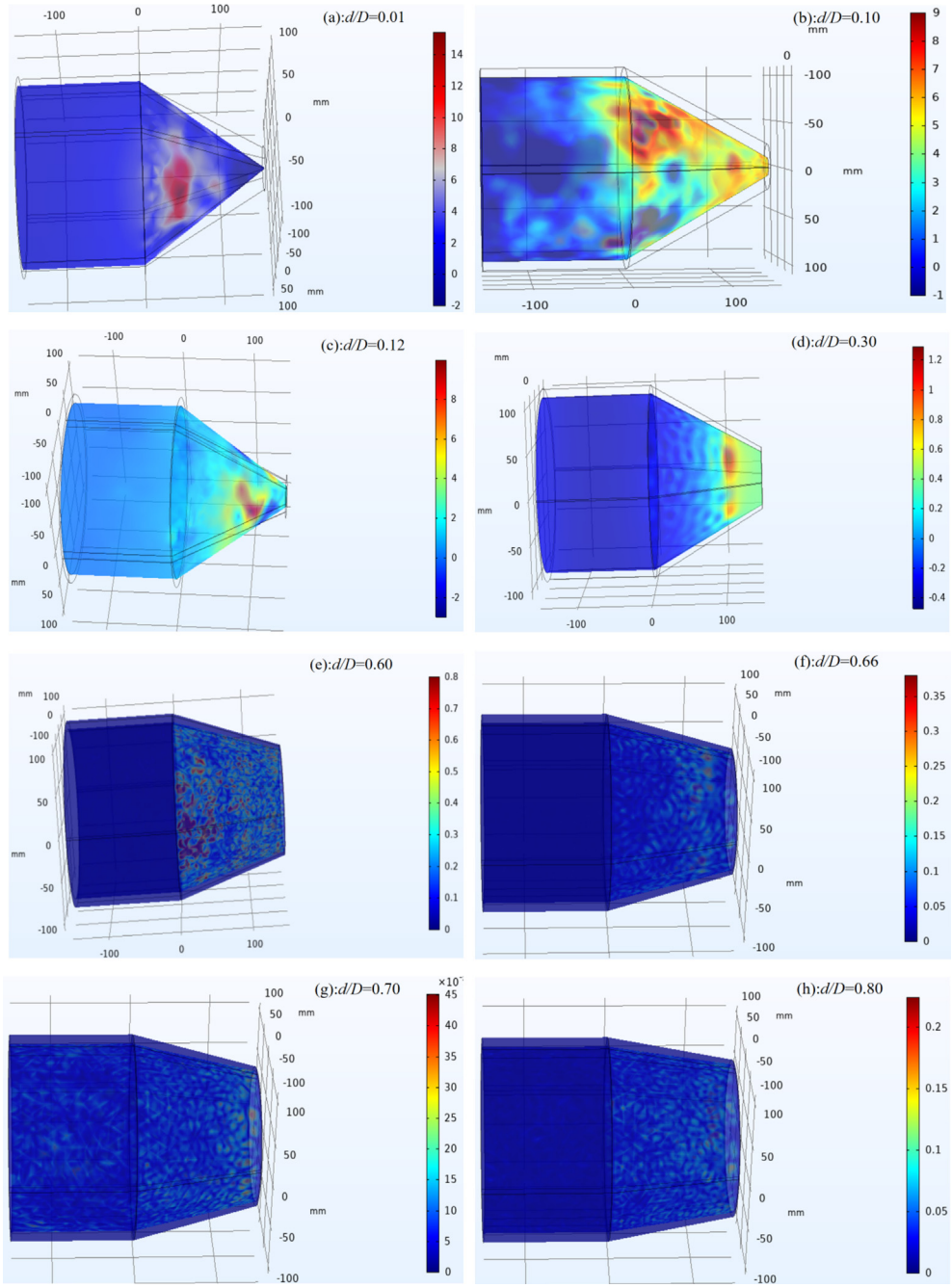

Fig. 4. The numerical sound field distribution results of ABHs under different tip diameters at 100 Hz (colour online).

are 150 mm. In this experiment, the samples are produced by 3D printing with resin material. The material parameters are as follows: the density is ρ = 1.18 × 10^3 kg/m^3, Young's modulus is 1 × 10^9N/m^2, and Poisson's ratio is 0.38.

The test frequency range of the standing wave tube is 50 Hz ~ 1.6 kHz. The inner diameter of the standing wave tube is 100 mm, so the diameter of the acoustic black holes is 99 mm. The gap between the acoustic black holes and standing wave tube is sealed with rubber cement, which meets the requirements for effective sealing. The sound absorption end of the standing wave tube has a sound absorption wedge. The sound insulation test error is 1 dB, ensuring the experiment's accuracy.

The experimental acoustic transmission loss (*STL*) data of the three samples are shown in Fig. 8. The lowest *STL* value in the test samples appears at 32 Hz, and the lowest *STL* value of the ABH with a tip diameter of 12 is 11 dB. As the tip diameter decreases, the low-frequency *STL* increases, which shows that the smaller the ABHs' tip diameter, the higher the *STL*, and more acoustic low-frequency waves are focused in the ABHs. This demonstrates that reducing the tip diameter *d* can improve the *STL* and sound insulation performance of ABHs at low frequencies.

We converted the *STL* into a transmission coefficient t_w to study the acoustic transmission characteristics of the test samples. The *STL* formula is:

$$STL = -10\log_{10}(\frac{E_T}{E_i}) = -10\log_{10}(t_w) \tag{16}$$

The expression of transmission coefficient t_w is:

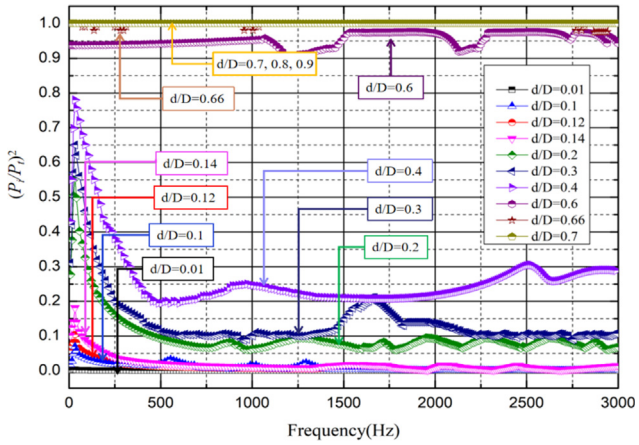

Fig. 5. The numerical results of the transmission coefficients of ABHs with different tip diameters (colour online).

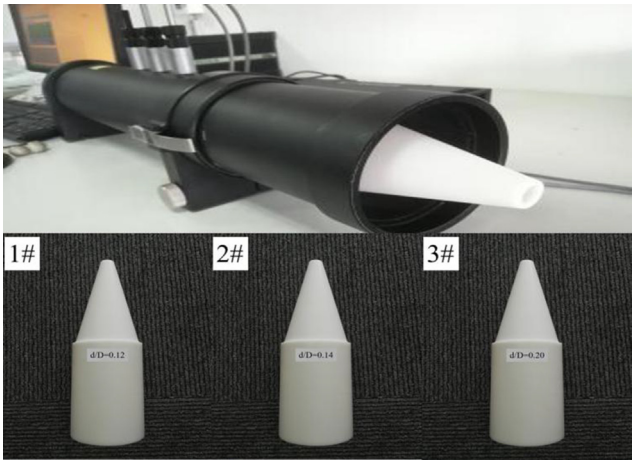

Fig. 7. Standing wave tube testing system and the tested ABHs (colour online).

$$t_w = 10^{-\frac{STL}{10}} \tag{17}$$

The acoustic transmission coefficients of the three test samples are obtained using Eq. (17) as shown in Fig. 9. The largest transmission coefficient value t_w in the test samples still appears at 32 Hz, and the lowest t_w value of the ABH with a tip diameter of 12 is only 0.09, demonstrating that 91% of the sound waves in the test frequency band can be isolated. When the tip diameter increases from 0.12 to 0.2, the transmission coefficient increases from 0.09 to 0.6 at 32 Hz. This significant change indicates that a small change in the tip diameter d has a significant impact on the transmission performance of ABHs at very low frequencies (below 150 Hz).

The logarithmic relationships of sound transmission coefficients with different tip diameters d are plotted at 48 Hz, 96 Hz, 152 Hz, and 200 Hz. Fig. 10 demonstrates that the curves of the sound transmission coefficients at these frequencies fully coincide with the line of the slope of 3. The results show that the acoustic transmission coefficient t_w is proportional to the 3 power of the tip diameter d at low frequencies. The experimental results also fully verify the accuracy of Eq. (12) obtained using our theorical method.

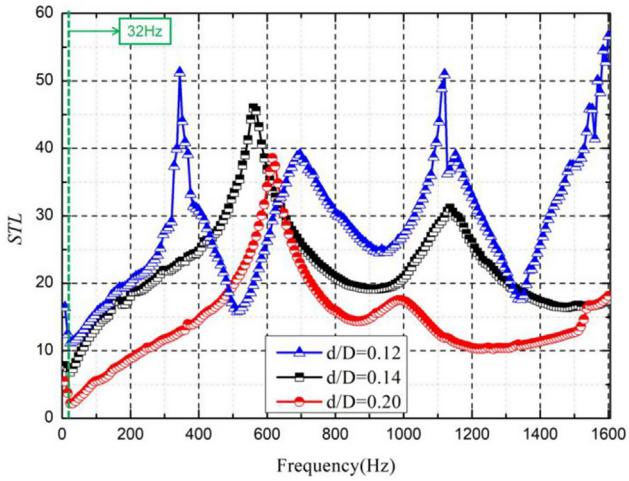

Fig. 8. Experimental data on the sound transmission loss (*STL*) of the tested samples (colour online).

5. Summary and conclusions

In summary, we have characterised the spontaneous catastrophe sound energy flux in ABHs at low frequencies and obtained the quantitative relationships of the two stable phases in this phase transition, which accurately agreed with both the experimental and numerical data. According to the sound wave deceleration in the ABHs, we analysed the mechanism of the sound energy-focusing effects and thoroughly explored the spontaneous catastrophe behaviour of sound energy flux caused by the sound energy-focusing effects. The theoretical analysis shows that there are two catastrophe behaviours in this phase transition that are caused by decreasing the tip diameter of the ABHs, resulting in

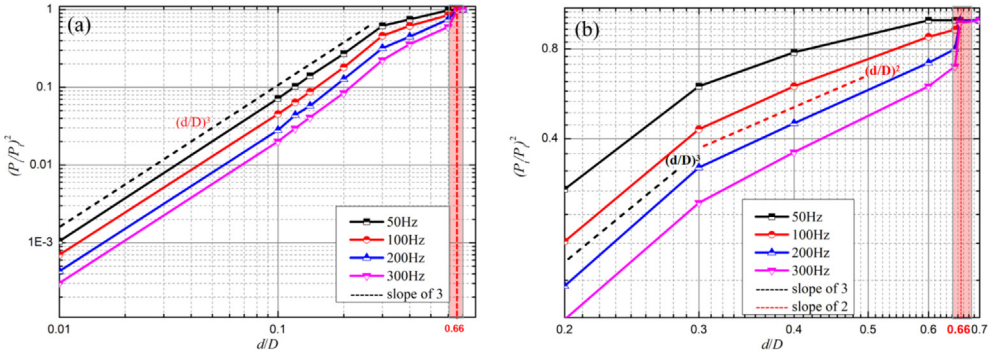

Fig. 6. The numerical results of the relationship between the transmission coefficients $(P_t/P_i)^2$ of the ABHs and tip diameter d (colour online).

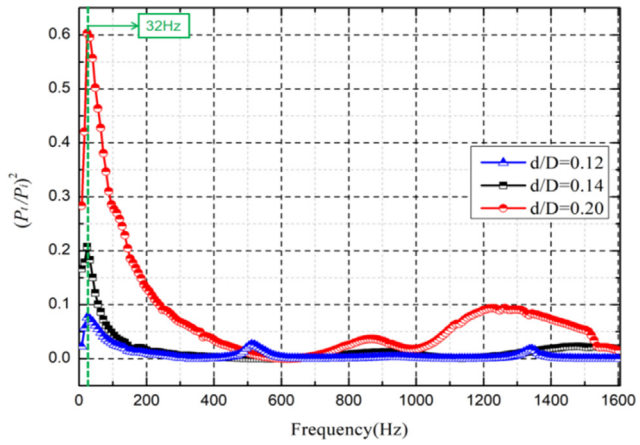

Fig. 9. Experimental data of the transmission coefficients of the tested samples (colour online).

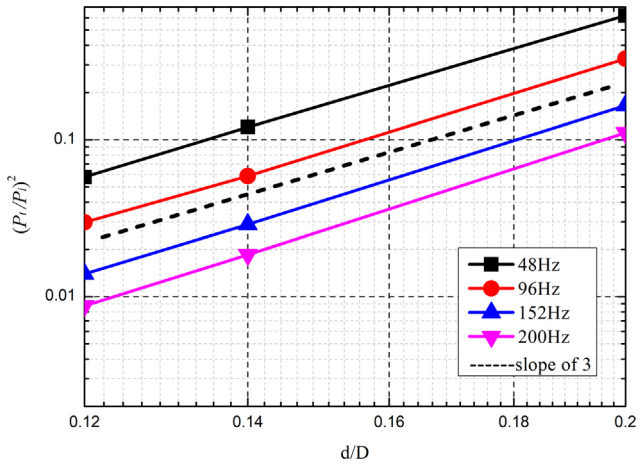

Fig. 10. Logarithmic relationship between the tested transmission coefficients and tip diameter *d* (colour online).

first-order phase transitions. The acoustic energy transmitted from the tip of the ABHs is proportional to the 3 power law and square of the tip diameter *d*, which was verified by our numerical method, and the 3 power law of *d* was also observed in our experimental results. Our experiments and simulation methods proved the catastrophe sound energy behaviour in the ABHs and the quantitative relationships obtained during the phase transitions.

For sound insulation engineering applications, ABHs with a tip diameter of 12 mm can isolate more than 11 dB of low-frequency sound waves below 1600 Hz, and the sound insulation coefficient can be further increased by reducing the tip diameter. Therefore, reducing the tip diameter of ABHs can improve the sound insulation coefficients at low frequencies.

CRediT authorship contribution statement

Xiao Liang: Conceptualization, Methodology, Software. **Jiaming Chu:** . **Jiale Tan:** Validation, Software. **Songhui Nie:** Validation. **Baixi Liu:** Writing - review & editing, Supervision, Data curation. **Xuejun Zheng:** Writing - review & editing. **Zhuo Zhou:** Writing - review & editing. **Jiu Hui:** Writing - review & editing.

Declaration of Competing Interest

The authors declare that they have no known competing financial interests or personal relationships that could have appeared to influence the work reported in this paper.

Acknowledgements

This study was supported by the Guangdong Basic and Applied Basic Research Fund Regional Joint Fund Youth Fund Project under grant no. 2019A1515111118, the Xiangtan Joint Fund Project of the Natural Science Foundation of Hunan Province under grant no. 2020JJ6032 and the Hunan Innovative Province Construction Special Major Landmark Innovation Demonstration Project Changsha Zhuzhou Xiangtan Landmark Engineering Technology Project under grant no. 2019XK2303.

References

[1] Bowyer EP, Krylov VV. Damping of flexural vibrations in turbofan blades using the acoustic black hole effect. J Appl Acoust 2014;76:359–65. https://doi.org/10.1016/j.apacoust.2013.09.009.
[2] Horstmann B, Reznik B, Fagnocchi S, Cirac JI. Hawking radiation from an acoustic black hole on an ion ring. J Phys Rev Lett 2010;104(25). https://doi.org/10.1103/PhysRevLett.104.250403.
[3] Cardoso V, Lemos J, Yoshida S. Quasinormal modes and stability of the rotating acoustic black hole: Numerical analysis. J Phys Rev D 2004;70(12):. https://doi.org/10.1103/PhysRevD.70.124032124032.
[4] Tang L, Ji H, Qiu J. Enhanced acoustic black hole effect using a modified thickness profile. C Inter-noise & Noise-con Congress & Conference 2016.
[5] Krylov V. Conditions for validity of the geometrical-acoustics approximation in application to waves in an acute-angle solid wedge. J Soviet Phys Acoust 1989;35(2):176–80. https://doi.org/10.3397/1.2827731.
[6] Krylov V. Localized acoustic modes of a quadratically-shaped solid wedge. J Moscow Univ Phys Bullet 1990;45(6):65–9.
[7] Gao N, Wu J, Lu K, Zhong H. Hybrid composite meta-porous structure for improving and broadening sound absorption.J. Mech Syst Sig Process 2021;154:107504. https://doi.org/10.1016/j.ymssp.2020.107504.
[8] Gao N, Luo D, Cheng B, Hou H. Teaching-learning-based optimization of a composite metastructure in the 0–10 kHz broadband sound absorption range. J Acoust Soc Am 2020;148(2):EL125–9. https://doi.org/10.1121/10.0001678.
[9] Gao N, Lu K. An underwater metamaterial for broadband acoustic absorption at low frequency. J Appl Acoust 2020;169:107500. https://doi.org/10.1016/j.apacoust.2020.107500.
[10] Bowyer EP, Krylov VV. Slots of power-law profile as acoustic black holes for flexural waves in metallic and composite plates. J Struct 2016;6:48–58. https://doi.org/10.1016/j.istruc.2016.02.002.
[11] Gao N, Tang L, Deng J, Kuan Lu, Hou H, Chen K. Design, fabrication and sound absorption test of composite porous matamaterial with embedding I-plates into porous polyurethane. J Appl Acoust 2020;175:. https://doi.org/10.1016/j.apacoust.2020.107845107845.
[12] Gao N, Guo X, Deng J, Cheng B, Hou H. Elastic wave modulation of double-leaf abh beam embedded mass oscillator. J Appl Acoust 2021;173:107694. https://doi.org/10.1016/j.apacoust.2020.107694.
[13] Foucaud S, Michon G, Gourinat Y, Pelat A, Gautier F. Artificial cochlea and acoustic black hole travelling waves observation: Model and experimental results. J Sound Vib 2014;333(15):3428–39. https://doi.org/10.1016/j.jsv.2014.03.016.
[14] Ouahabi AE, Abdelhalim VV, et al. Experimental investigation of the acoustic black hole for sound absorption in air. C 22nd International Congress on Sound and Vibration, 2015.
[15] Guasch O, Sánchez-Martín P. Transfer matrices to analyze the acoustic black hole effect in duct terminations. C Inter-noise & Noise-con Congress & Conference 2016.
[16] Aklouche O, Pelat A, Maugeais S, Gautier F. Scattering of flexural waves by a pit of quadratic profile inserted in an infinite thin plate.J. J Sound Vib 2016;375:38–52. https://doi.org/10.1016/j.jsv.2016.04.034.
[17] Cross M, Hohenberg PC. Pattern formation outside of equilibrium. J Rev Mod. Phys. 1993;65(3):851–1112. https://doi.org/10.1103/revmodphys.65.851.
[18] Cross M, Hohenberg PC. Spatiotemporal chaos. J Sci 1994;263(5153):1569–70. https://doi.org/10.1126/science.263.5153.1569.

[19] Dennin M, Ahlers G, Cannell DS. Spatiotemporal chaos in electroconvection. J Sci 1996;272(5260):388–90.
[20] Egolf DA, Greenside HS. Relation between fractal dimension and spatial correlation length for extensive chaos. Nature 1994;369(6476):129–31. https://doi.org/10.1038/369129a0.
[21] Bohr T, Bosch E, van de Water W. Spatiotemporal chaos. J Nature 1994;372:48. https://doi.org/10.1038/372048a0.
[22] Bohr T, Jensen MH, Paladin G, et al. Dynamical Systems Approach to Turbulence: Chaotic diffusion. UK: Cambridge University Press, Cambridge University Press; 1998. p. 370.
[23] Shraiman BI, Pumir A, van Saarloos W, Hohenberg PC, Chaté H, Holen M. Spatiotemporal chaos in the one-dimensional complex Ginzburg-Landau equation.J Physica D. Nonlinear Phenomena 1992;57(3-4):241–8. https://doi.org/10.1016/0167-2789(92)90001-4.
[24] Wang M, Wang X, Wang C, Xia Z, Zhao H, Gao S, et al. Spatiotemporal chaos in cross coupled map lattice with dynamic coupling coefficient and its application in bit-level color image encryption. J Chaos, Solitons Fractals 2020;139:110028. https://doi.org/10.1016/j.chaos.2020.110028.
[25] Liang X, Wu JH, Zhou G. Quantitative analysis for acoustic characteristics of porous metal materials by improved Kolmogorov's turbulence theory. J Appl Acoust 2018;130:210–5. https://doi.org/10.1016/j.apacoust.2017.09.019.
[26] Golubitsky M. An introduction to catastrophe theory and its applications. SIAM Rev 1978;20(2):65–100. https://doi.org/10.1137/1020043.